LBL-20749

Lawrence Berkeley Laboratory
UNIVERSITY OF CALIFORNIA

Physics Division

Presented at the 1985 SLAC Summer Institute on Particle Physics, Stanford, CA, July 29-August 9, 1985

HADRON PRODUCTION AT PEP/PETRA

H. Yamamoto

December 1985

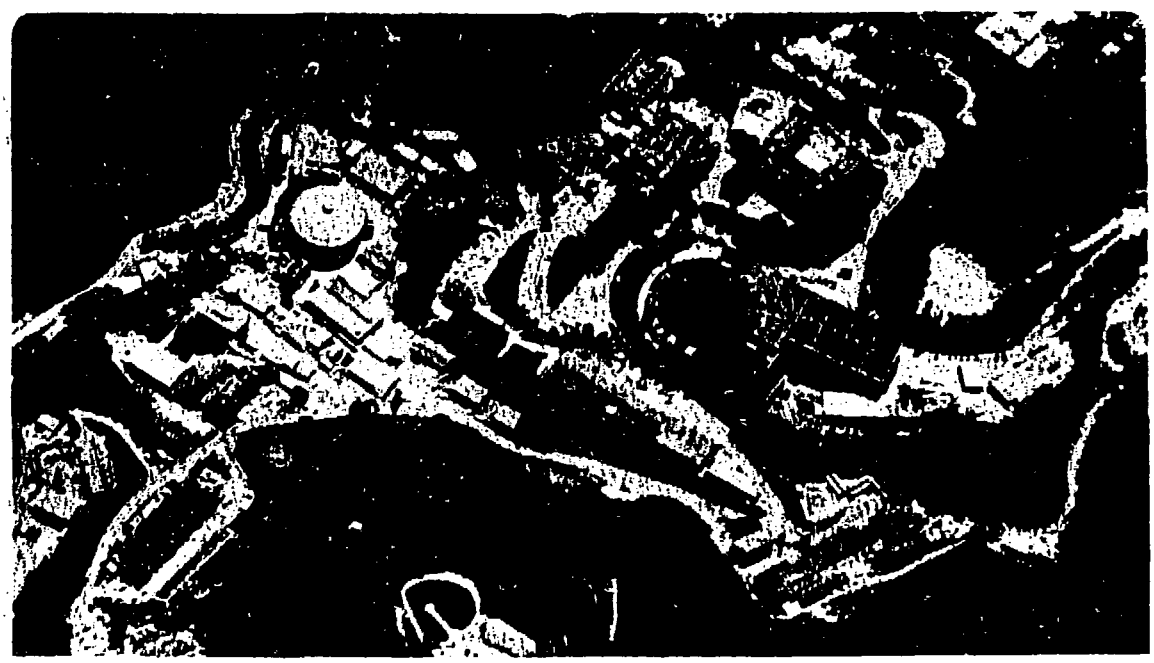

Prepared for the U.S. Department of Energy under Contract DE-AC03-76SF00098

LBL--20749

DE86 006335

Hadron Production at PEP/PETRA *

Hiroaki Yamamoto

Lawrence Berkeley Laboratory
University of California
Berkeley, California 94720

and

Department of Physics
University of Tokyo
Hongo, Bunkyo-ku, Tokyo

Abstract

Recent results on hadron production in e^+e^- annihilation at PEP and PETRA are summarized. The topics included are: 1) inclusive hadron production, 2) gluon vs quark jet, 3) analysis of 3 jet events and 4) $p - \bar{p}$ correlations. Experimental data are compared with predictions of several models to reveal underlying physics.

Talk presented at the
1985 SLAC Summer Institute on Particle Physics
Stanford, California
July 29 - August 9, 1985

*) This work was supported by the Department of Energy under contract numbers DE-AC03-76SF00098, DE-AM03-76SF00034, and DE-AC02-76ER03330, the National Science Foundation and the Joint Japan-US Collaboration in High Energy Physics.

DISCLAIMER

1 Introduction

Recent results on hadron production in e^+e^- annihilation at PEP and PETRA are summarized.[1] The main purpose of these experiments is to study the hadronization of partons in the framework of Quantum Chromodynamics (QCD).[2] Hadron production in e^+e^- annihilation is described in the following steps: 1) Annihilation of the electron and positron into a virtual photon or Z^0, 2) Production of a quark pair with virtuality of $O(\sqrt{s})$, 3) Radiation of partons from virtual partons, 4) Hadronization of partons with low virtuality, and 5) Decay of unstable particles.

The steps 1) to 3) can be calculated by QCD and the Weinberg-Salam model[3] of the electro-weak interaction, because perturbative expansion is known to work well in QCD for the large Q^2 region. In the region of small Q^2, however, QCD perturbation fails, and the hadronization of partons, step 4), is not calculable. Therefore, main problems to be studied are: i) confirmation of the Weinberg-Salam model and QCD in the perturbative region, ii) at what value of Q^2 and how does the perturbative phase merge to the non-perturbative phase in QCD ? and iii) how do partons hadronize ?

In the analysis, several models for perturbative and non-perturbative regions are combined and experimental data are compared with model predictions to test which model is appropriate to describe the data. An abrupt transition from perturbative phase to non-perturbative phase is assumed in these models.

Two methods exist to calculate QCD perturbatively. A) Perturbative expansion in powers of α_S, the strong coupling constant: the cross sections for parton production in e^+e^- have been calculated up to α_S^2.[4] The results depend on the scheme used to regularize perturbative singularities. Calculations of exact matrix elements to higher orders are very difficult. B) The

Leading-collinear Logarithmic Approximation (LLA), which supplements the above exact expansion in α_S.[5] The LLA method permits emission of as many partons as are kinematically allowed. The LLA cross sections are only approximate, however, and some cross sections are not given correctly, e.g., the 3 jet cross section with small thrust.

At the termination of the perturbative phase, the parton system must be converted to a hadronic system. Several models have been proposed to describe the hadronization process based on the general arguments of QCD.[6] The most popular models are: a) Independent Fragmentation Model (IF) (Fig.1 (a)) [7,8,9], b) String Fragmentation Model (SF) (Fig.1 (b))[10], and c) Cluster Fragmentation Model (CF) (Fig.1 (c)) [11,12,13]. Basic assumptions of these models are as follows:

a. In the IF model, each parton is assumed to fragment independently based on the Field-Feynman mechanism[7]. The hadrons produced from a parton are distributed cylindrically around the parent parton direction. A serious problem with this model is that the 4 momentum and flavor conservation is imposed in an ad-hoc manner.

b. In the SF model, it is assumed that strings are stretched between partons along the direction of color flow. This assumption is based on the string picture of confinement. Each string is assumed to hadronize with cylindrical symmetry in its rest frame. Hadrons are boosted to the e^+e^- CM frame if the CM frame and the string rest frame differ. An important consequence of this Lorentz boost is that in 3 jet events, interpreted as $q\bar{q}g$, more hadrons are produced in the regions between $q-g$ and $\bar{q}-g$ than in that between $q-\bar{q}$. In this model, the 4 momentum and flavor are naturally conserved. Recent studies have shown that the hadron state produced from two partons with a

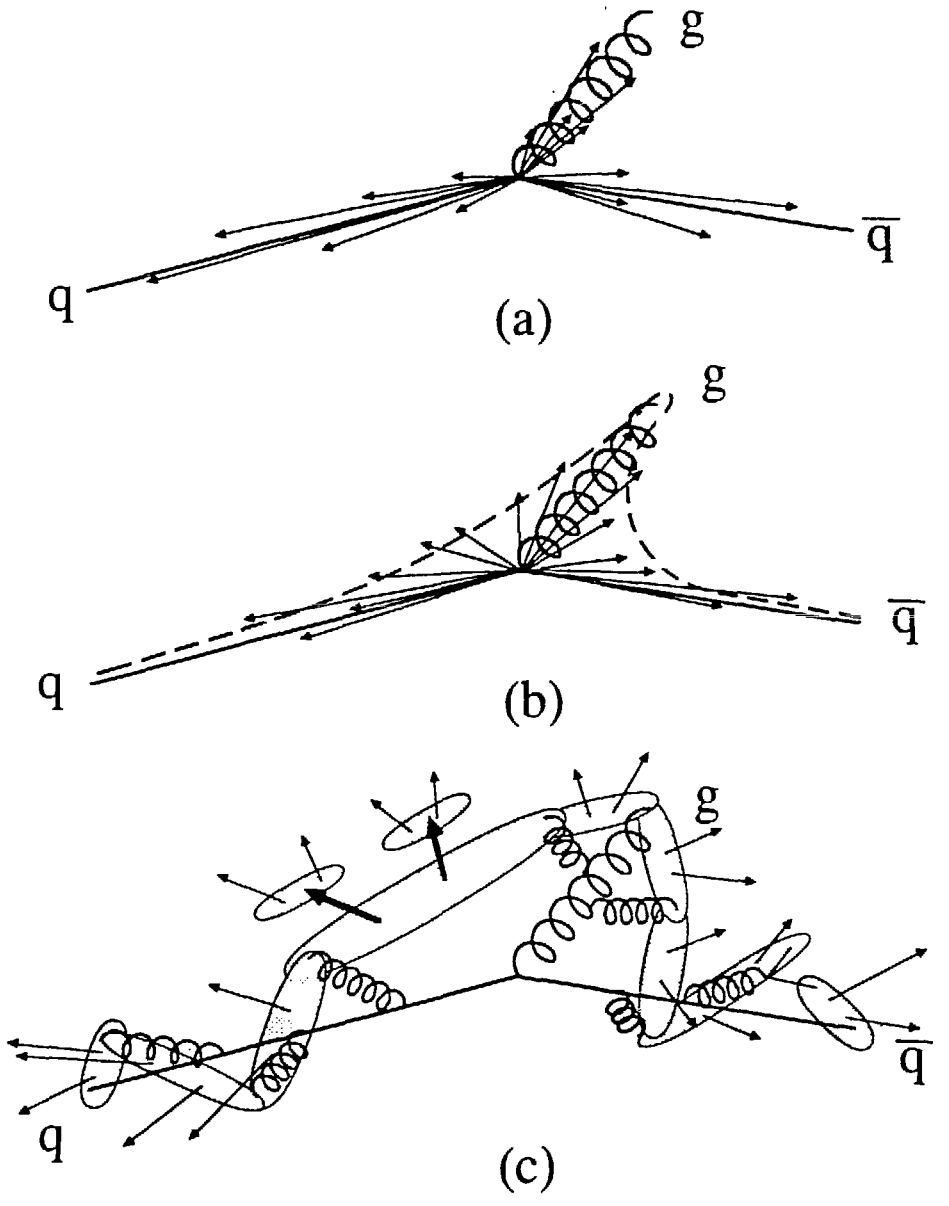

Fig. 1. Schematic representations of a 3 jet event in (a) the Independent Fragmentation Model, (b) the String Fragmentation Model and (c) the Cluster Fragmentation Model.

small invariant mass is almost the same as the hadron state produced from a single parton with the same momentum in this model.[14] This is an attractive feature because it reduces the dependence of model predictions on the perturbative cutoff scheme.

c. The CF model is used with the LLA method. The invariant mass of two neighboring partons after the parton shower evolution by LLA is rather small, $O(1GeV)$, of the scale of hadronic masses. Based on the scheme of preconfinement, it is assumed that color singlet clusters are formed from neighboring partons. Each cluster is viewed as a heavy resonance with a large decay width. Each cluster is assumed to decay into two body states, while the flavors of the decay products are determined by their phase space and spin freedom.[15]

The IF and SF models are the two extreme cases. In the former, the interaction between partons is assumed to be negligible until the end of the hadronization process, while in the latter, maximal interaction between partons through strings is assumed. The CF model where a parton shower is generated by LLA lies between IF and SF. For hadron production in the central region, it is similar to the SF model, but in the high momentum region, it predicts hadronization to proceed independently.

In the following, experimental data are compared with several Monte Carlo predictions to test these assumptions. The principal Monte Carlo programs are:

1. The Hoyer Monte Carlo[9] and the Ali Monte Carlo[8], which uses QCD matrix element up to $O(\alpha_S^2)$ and IF.

2. The LUND Monte Carlo[10], which uses QCD matrix element up to $O(\alpha_S^2)$ and SF.

3. The Webber Monte Carlo[12] and the Gottschalk Monte Carlo[13], which use the LLA and CF. The Webber Monte Carlo, in addition, includes a part of the next leading order corrections, i.e. the soft gluon interference effect.[16]

Recent experimental data from PEP and PETRA are presented in the following sections, and they are used to study the problems mentioned above. In Section 2, inclusive particle production data are summarized, together with analyses of the flavor dependence of the hadronization process. In Section 3, gluon jets are compared with quark jets. The differences between the particle spectra in gluon jets and that in quark jets are used to study the higher order effects neglected in the 2nd order QCD. The 3 jet events are used to evaluate the SF model and the IF model in Section 4. The effect of the soft gluon is also discussed in this section. Correlations between a proton and an antiproton are used to test various baryon production models in Section 5. In the last section, the summary of the talk is given.

2 Inclusive Hadron Production

2.1 Ordinary hadron production

Most low lying ordinary hadrons, which contain only u, d and s quarks, have been observed in e^+e^- experiments. Figure 2 shows the multiplicities of ordinary hadrons measured by PEP and PETRA experiments.[17] Only those data taken in the full or nearly full momentum range are included in the figure. Recently, ARGUS has observed hyperon production at 10 GeV of Σ^*, Ξ^* and Ω^-.[18] Figure 3 shows production cross sections of $K^\pm$ and Λ measured by many groups.[19] As can be seen from Fig.2 and Fig.3, data from different groups are quite consistent, with a few minor exceptions.

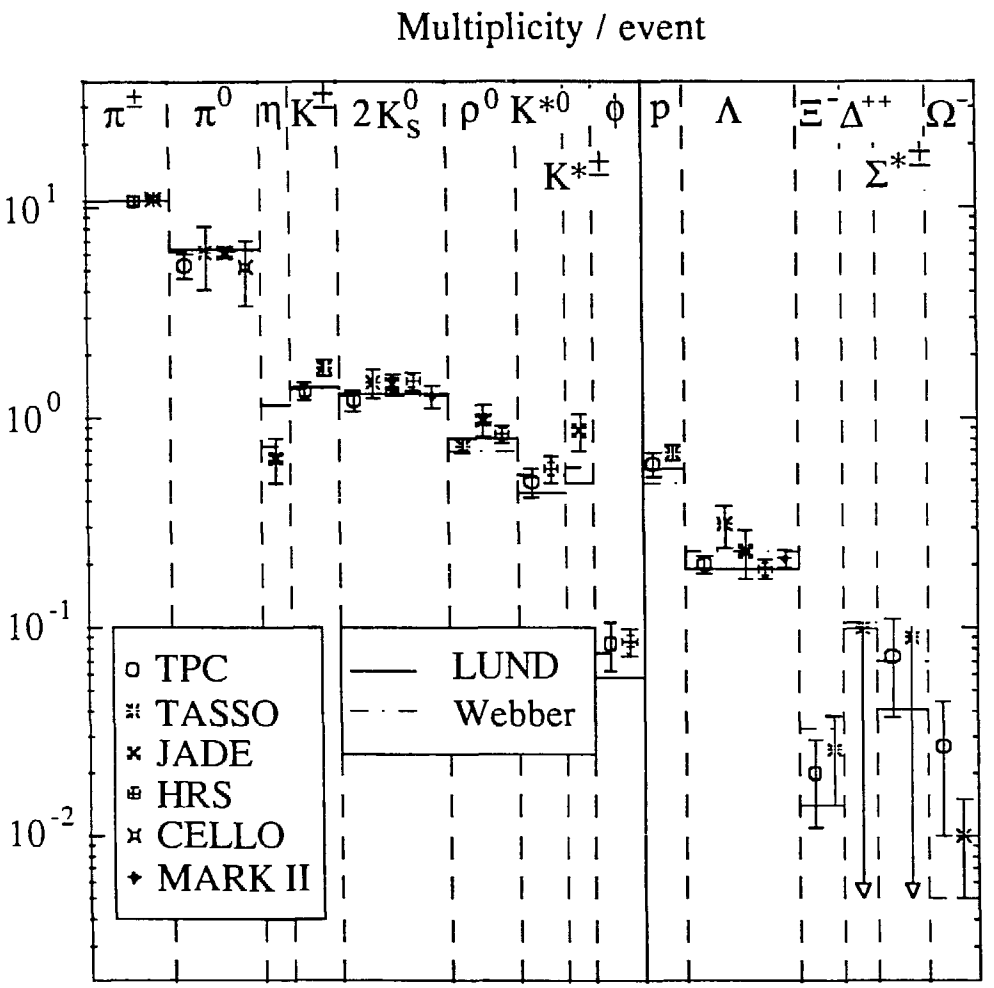

Fig. 2. Ordinary hadron multiplicities measured by PEP and PETRA experiments compared with Monte Carlo predictions.

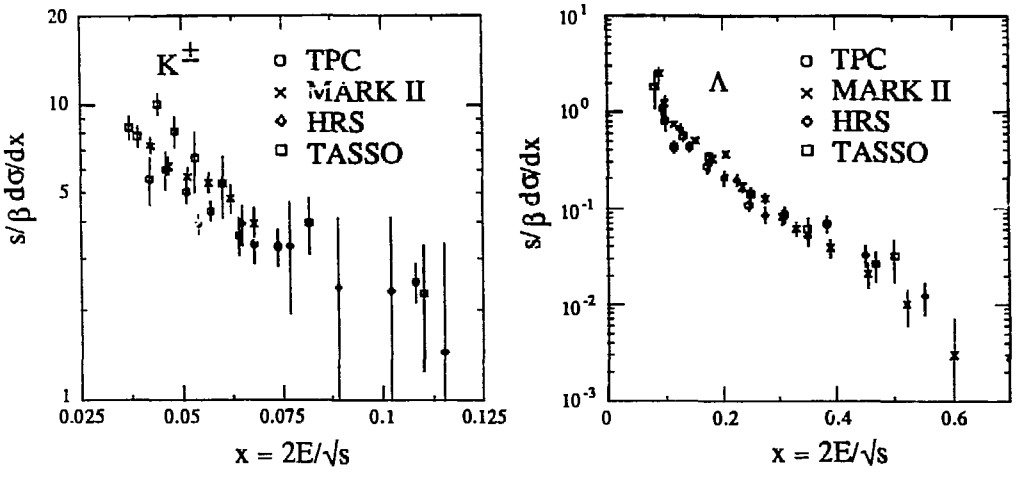

Fig. 3. Inclusive cross sections of $K^{\pm}$ and Λ at PEP and PETRA.

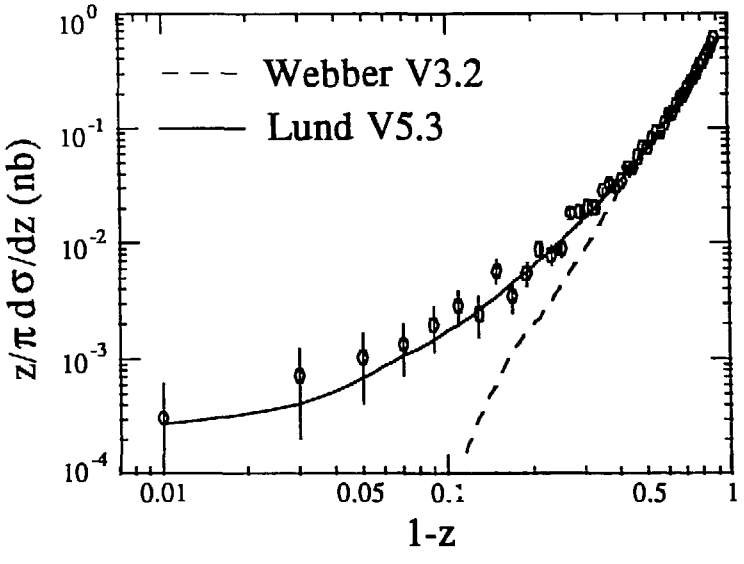

Fig. 4. HRS measurment and Monte Carlo predictions of the charged particle cross section at high z.

In Fig.2, the predictions of the Lund SF and Webber CF models are also shown. The two models are in reasonable agreement with observed multiplicities and single particle cross sections, despite the very different manners in which the relative abundance and the spectrum shape are determined.

In the Lund model, the production rate of a hadron with a given flavor is mainly determined by the rates of quark-antiquark and diquark-antidiquark pair production in the string-like color field. The physical motivation comes from 2-dimensional field theory, but several phenomenological parameters have been introduced, which are to be determined by experimental data. For example, the s/u ratio (ratio of $s\bar{s}$ to $u\bar{u}$ pair production rates) is determined from the ratio of multiplicities for kaons and pions. Parameters in the fragmentation function should be determined by the measured momentum spectrum. The fragmentation function proposed by the LUND group can predict the mass dependence of the function. Once the parameters are determined by the charged particle distribution, the model can predict the momentum spectra of charm and bottom particles.[20] This prediction of the mass dependence is consistent with experimental data.

In the Webber model, the differential cross section is determined in two steps. First, parton configurations are generated in momentum space in LLA, and the mass and momentum of color singlet clusters are determined. Next, these clusters decay to hadrons governed only by kinematical factors, i.e., phase space and spin factors.

The charged particle cross section in the high z region ($z = E_{had}/E_{beam}$) has been measured by HRS at PEP.[21] (Fig.4) The cross section in this region is very interesting because 1) the contribution of the decay products from resonant particles is small, and 2) the behavior of the cross section is strongly model dependent at around $z = 1$. Such a measurement is only

possible with their good momentum resolution, $\Delta p/p = 0.25\% p(GeV/c)$ at $p_{had} = E_{beam}$. The number of background events above $z = 0.9$ is estimated to be less than 0.1.

In Fig.4, the predictions of the LUND MC and the Webber MC are also shown. As can be seen, the LUND MC gives a good description of the data, but the Webber MC predicts too soft a momentum spectrum above $z = 0.6$. In order to trace back the origin of this problem in the Webber MC, another combination of assumptions was tested in which the perturbative phase is based on LLA (as before) but the hadronization phase is based on SF. This model gives almost the same result as the LUND MC. Failure of the Webber MC in the high z region is now explained by the fact that the cluster is forced to decay into two hadrons. It is then difficult to produce a high z hadron, even if the energy of the cluster is approximately equal to the beam energy. This difficulty is common to hadronization schemes based on cluster decay. If a cluster with small invariant mass is replaced by a hadron with a mass close to the cluster mass, the predicted spectrum becomes harder.[22]

2.2 Charm particle production

The $D^{*\pm}$ provides a unique tool for measuring the fragmentation function of the c quark. The $D^{*\pm}$ cross sections measured by DELCO, HRS, TPC, JADE and TASSO at around $E_{CM} = 30\ GeV$ are shown in Fig.5.[23] The absolute value of the production cross section depends on the branching fractions of the D meson. In this regard, the fact that the latest MARK III data[24] significantly differs from the values in the Particle Data Table[25] affects the production cross section. The cross section given here will become smaller if the new branching fractions are used.

The cross sections of Λ_c measured by CLEO at CESR and ARGUS at

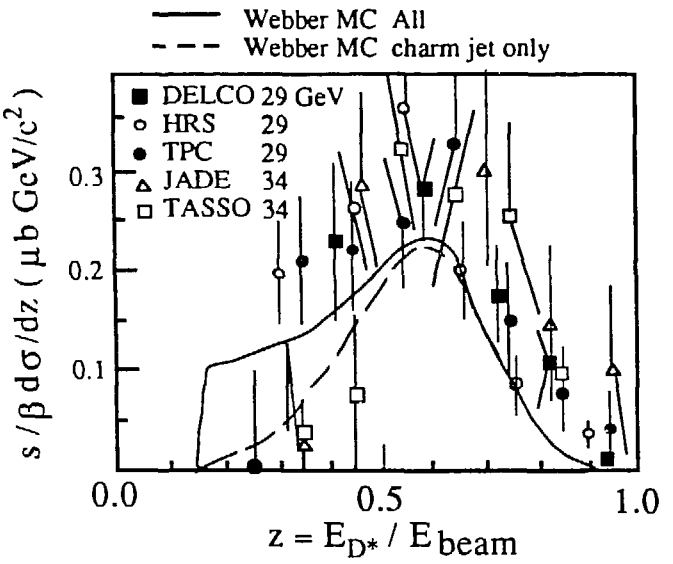

Fig. 5. Cross sections of D* measured at PEP and PETRA. Also shown are Webber MC predictions.

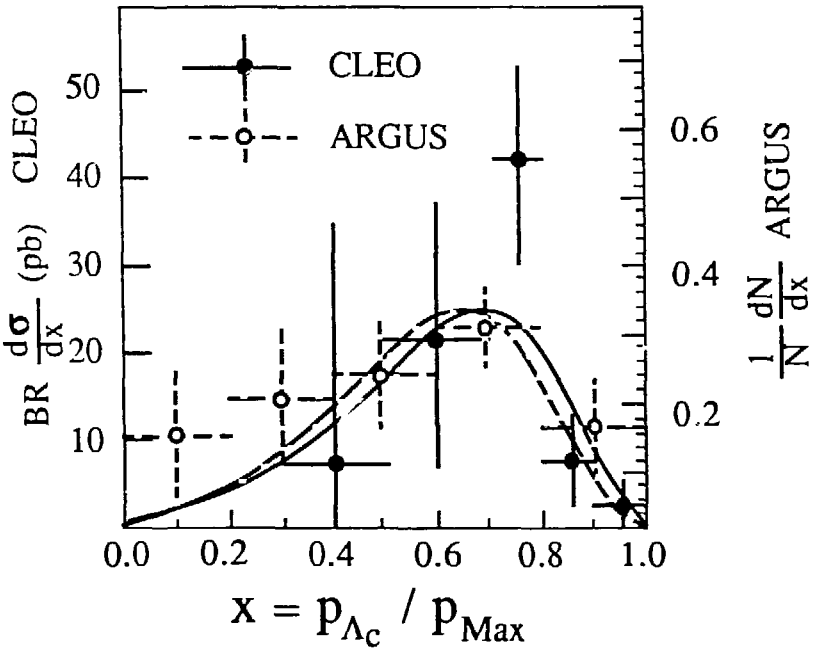

Fig. 6. Momentum distributions of Λ_c measured by CLEO and ARGUS. The solid line is the Peterson function fitted to CLEO D* data and the broken line is the same function fitted to the ARGUS data.

DORIS II are shown in Fig.6. The solid line in this figure is the Peterson function[27] with $\epsilon = 0.14$, fitted to the D* spectrum obtained by CLEO, and the broken line is the same function with $\epsilon = 0.21$, fitted to the Λ_c spectrum of ARGUS. No difference is observed between the D* spectrum and Λ_c spectrum. As is clear from Fig.4, Fig.5 and Fig.6, the spectrum is harder for charm particles than for ordinary hadrons.

The observed hadron spectrum deviates from the fragmentation function at the parton level due to radiative corrections, multi-jet emissions and kinematics. The scaled momentum $< z >$ after unfolding these effects has been calculated by S. Bethke, and it has been shown that $< z >$ is almost independent of E_{CM} in the range of $10 - 34\ GeV$.[28] The average value of z was found to be $0.71 \pm 0.014 \pm 0.03$.

In Fig.5, predictions of the Webber MC are also shown. The solid line is the prediction including all contributions and the broken line gives the distribution of D* in $c\bar{c}$ events. In the Webber model, the fragmentation function is not given externally but is determined by dynamics (LLA) and kinematics (masses of quarks and hadrons). The flavor dependence of the inclusive spectrum comes mainly from the differences in quark mass. The Webber MC predicts too soft a spectrum in the high z region, but the spectrum around $z = 1$ depends strongly on the assumptions made for the production of heavier resonances, e.g., D**.

2.3 Flavor dependence of the hadronization process – u,d,s vs c,b jets

As has been shown above, the spectrum of charm particles is harder than that of ordinary hadrons. This difference was predicted based on kinematics due to the difference of the quark mass.[29] Therefore, the test of the flavor

dependence of the hadronization process should be addressed as follows: 1) Is the hadronization dependent on the quark flavor for that part excluding the leading part ?, and 2) is the quark-gluon coupling dependent on the quark flavor ? Here, leading part means those hadrons which are decay products of hadrons which contain the primary quarks.

The flavor dependence of the charged multiplicity has been tested by MARK II. They used prompt leptons to enrich c and b jets by requiring $p \geq 2GeV/c$ and $p_t < 1\ GeV/c$ (for charm), and, $p \geq 2\ GeVc$ and $p_t \geq 1\ GeV/c$ (for bottom).[30] The average total charged multiplicities in $Q-\overline{Q}$ jets obtained in this analysis are $16.1 \pm 0.5 \pm 1.0$ for bottom events and $13.2 \pm 0.5 \pm 0.9$ for charm events. The non-leading hadron multiplicity N_{NL} has been estimated by subtracting the average multiplicity of the leading part from the total multiplicity: $N_{NL}(bottom) = 5.2 \pm 0.5 \pm 0.9$ and $N_{NL}(charm) = 8.1 \pm 0.5 \pm 0.9$. The average invariant mass of the non-leading part, W_{NL}, and the mean energy fraction of the heavy hadron $< z >_Q$ are related by the following equation:

$$W_{NL} = E_{CM} \cdot (1 - 2 \cdot < z >_Q).$$

In Fig.7, the average charged multiplicity over a wide range of E_{CM} is shown. Assuming that the relation between N_{NL} and W_{NL} is the same as that between the average charged multiplicity and E_{CM}, they found the mean energy fraction of heavy hadrons $< z >_Q$ to be $< z >_b = 0.79^{+0.10}_{-0.05}$ and $< z >_c = 0.60^{+0.09}_{-0.11}$. These values are consistent with measurements based on lepton inclusive spectra and D* fragmentation.[23,30,31] Turning the argument around, one can conclude that the hadronization of the non-leading part is independent of the leading flavor.

Particle distributions of non-leading hadrons have been studied by several groups using particles in the side of the event opposite to the side of the

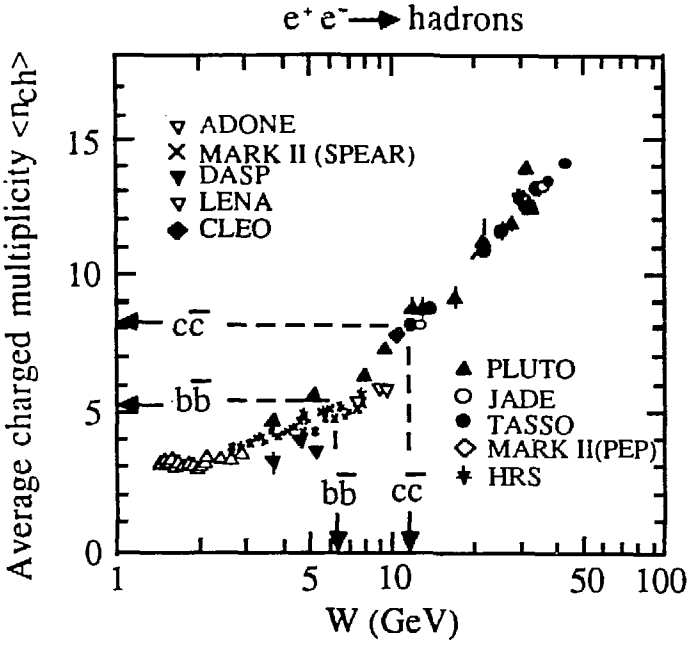

Fig. 7. The energy dependence of the charged multiplicity in e^+e^- annihilation. The arrows indicate the non-leading charged multiplicities for $b\bar{b}$ and $c\bar{c}$ events, and the corresponding invariant masses.

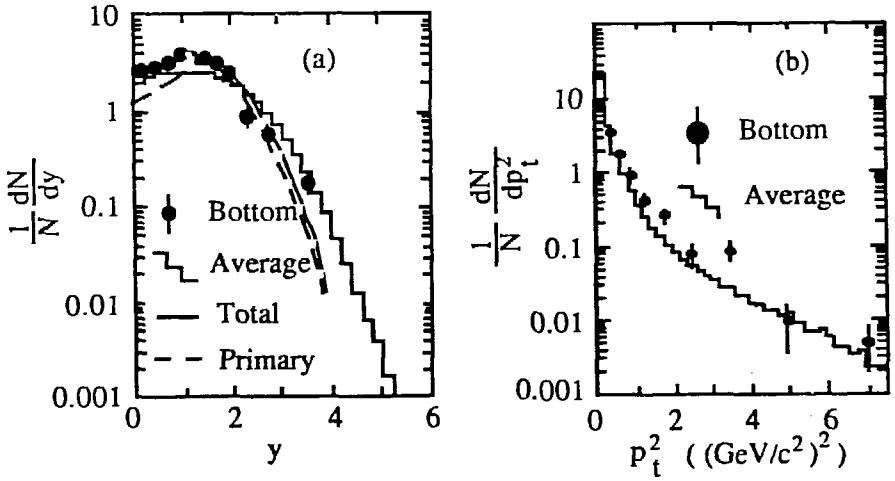

Fig. 8. (a) Rapidity and (b) transverse momentum distributions of charged particles in bottom and average jets measured by DELCO. The LUND MC predictions are given in (a) for total and for primary hadrons.

particle used to tag the specific quark type. In the following, the results reported by HRS (preliminary) for light quark jets vs charm jets[32] and by DELCO for average jets vs bottom jets[33] are presented.

HRS has used large momentum charged particles with $z > 0.7$ to tag light quark jets. The charm events are tagged by observing a peak in the D*-D mass difference, with assumed D decay modes of $D \to K\pi$ and $D \to K\pi\pi\pi$. For the 1st decay mode, the minimum z is required to be 0.4, while for the 2nd it is required to be 0.5. The average values of momentum and transverse momentum in these jets are $< p >_{charm} = 1.38 \pm 0.06\ GeV/c^2$, $< p >_{light} = 1.52 \pm 0.04$, $< p_t >_{charm} = 0.39 \pm 0.01$ and $< p_t >_{light} = 0.40 \pm 0.01$. No significant difference is observed between charm quark jets and light quark jets, except that the average momentum in charm jets is slightly softer than that in light quark jets. This result can be reproduced by models where the same hadronization scheme is used for light quark jets and charm quark jets.

DELCO has used electrons with $p = 0.5 - 5.5 GeV$ and $p_t > 1 GeV$ to tag bottom quark jets, and has compared those jets with jets in the their entire event sample. The rapidity and transverse momentum distributions in these two jet samples are shown in Fig.8(a) and (b). The average values of momentum and transverse momentum in these jets are $< p >_{bottom} = 1.06 \pm 0.04$, $< p >_{average} = 1.293 \pm 0.002$, $< p_t^2 >_{bottom} = 0.31 \pm 0.03$ and $< p_t^2 >_{average} = 0.274 \pm 0.001$. The observed rapidity distribution in the bottom quark jets is slightly softer than that in the average jets, and shows a dip at $y = 0$. In Fig.8(a), the LUND Monte Carlo predictions are also shown. In this model, the hadronization process is the same for all types of quark jets. The solid line shows the rapidity distribution of all particles and the broken line shows that of the leading part. The leading hadron distribution gives a clear dip at $y = 0$ due to kinematics, the large $< z >$ of

bottom hadrons and subsequent decays with high multiplicity. The solid line is consistent with the data, and the difference between the bottom jets and the average jets can be explained by the difference in the leading hadrons.

The test of the flavor dependence of α_S is made by TASSO, JADE and HRS by using charm events tagged by D*. TASSO found $\alpha_S(c) = 0.153 \pm 0.031 \pm 0.030$ and $\alpha_S(c)/\alpha_S(average) = 1.00 \pm 0.20 \pm 0.20$, using IF models for hadronization with 2nd order QCD calculation for the parton cross section. JADE obtained $\alpha_S(c) = 0.13 \pm 0.08$ using the LUND MC. HRS obtained $\alpha_S(c)/\alpha_S(u,d,s) = 1.03 \pm 0.27$ (preliminary)[36], where $\alpha_S(u,d,s)$ means the α_S measured for light quark jets tagged by large momentum charged particles. The quoted errors are statistical only. α_S measured for the charm quark is equal to α_S measured for average quarks[37] within statistics and no flavor dependence is observed.

3 Hadron spectrum in gluon jets and quark jets

The particle momentum spectra in gluon jets and in quark jets have been compared by MARK II.[38] The analysis uses charged particles and photons in 90000 events and proceeds as follows:

- 3 jet events are selected by using a cluster algorithm.
- The momentum of each jet is calculated by summing the momentum vectors of particles which belong to the jet. The energy of the jet is calculated from opening angles between jets assuming massless parton kinematics.
- Events with a nearly 3-fold symmetry are selected by requiring the

opening angles between any two jets to lie between 100° and 140°. A total of 560 events is selected to be used in the following analysis.

- The scaled momentum of each particle is defined to be $x_i = p_i/E_j$, where p_i is the momentum of particle i and E_j is the energy of the jet tc which it is assigned.

- The distribution in x is corrected for the detector acceptance and initial state radiation. This momentum distribution is viewed as the sum of the distributions in the one gluon jet and two quark jets with energy of $1/3E_{CM}$ each.

- The momentum distribution in events with two quark jets of energy $1/3E_{CM}$ each is calculated by interpoiation of existing data at several different energies. Most events in these samples are 2 jet events and can b- used to approximate the particle distribution for 2 jet events. The broken line in Fig.9(a) is the distribution obtained by this interpolation.

- The scaled momentum distribution in gluon jets is calculated by the following equation.

$$\begin{aligned} \frac{1}{\sigma_{tot}}\frac{d\sigma}{dx}(gluon\ jet) &= \frac{1}{\sigma_{tot}}\frac{d\sigma}{dx}(3\ jet\ events, E_{CM} = 29GeV) \\ &- \frac{1}{\sigma_{tot}}\frac{d\sigma}{dx}(2\ jet\ events, E_{CM} = 19.3GeV) \end{aligned}$$

- The ratio $r(x)$, which approximates the ratio of $\frac{1}{3}(gluon\ jet + 2 \cdot quark\ jet)\ /\frac{1}{2}(2 \cdot quark\ jet)$, is defined as follows

$$r(x) = \frac{\frac{1}{3\sigma_{tot}}\frac{d\sigma}{dx}(3\ jet\ events, E_{CM} = 29GeV)}{\frac{1}{2\sigma_{tot}}\frac{d\sigma}{dx}(all\ events, E_{CM} = 19.3GeV)}$$

Figures 9(a) and (b) show the results for $1/\sigma_{tot} \cdot d\sigma/dx(gluon\ jet)$ and $r(x)$, respectively, along with the predictions of several Monte Carlo programs.

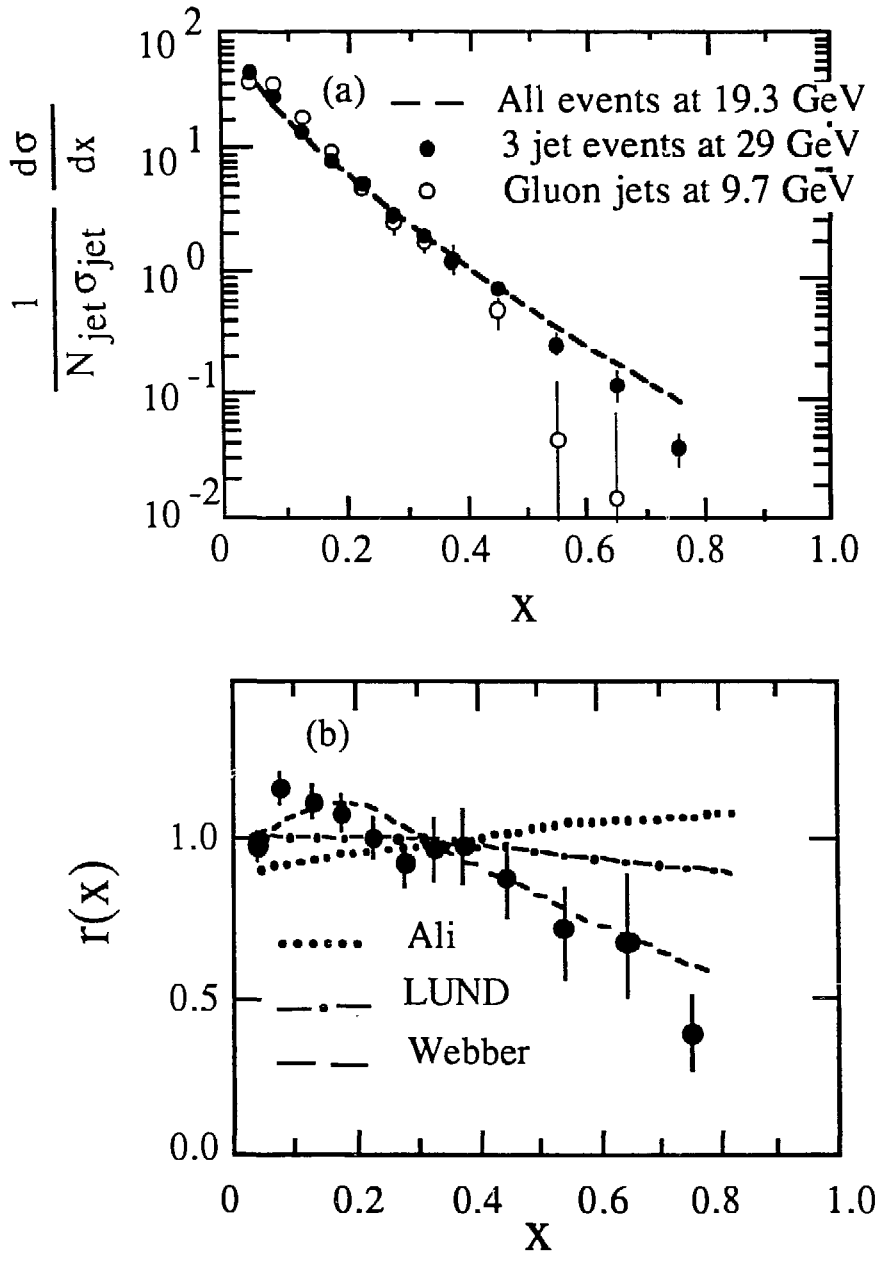

Fig. 9. (a) The charged particle distribution in 3-fold symmetric 3 jet events in comparison with that in hadronic events at 9.7 GeV. The distribution in gluon jets at 9 GeV mentioned in the text is shown by open circles. (b) The ratio $r(x)$ defined in the text as a function of x, with several Monte Carlo predictions.

The cross sections in Fig.9(a) are normalized by the number of jets in the events, N_{jet}, to give the distribution per jet. In Fig.9(a), black circles denote the distribution of particles in 3 jet events, while the white circles correspond to the distribution in gluon jets defined above. By comparing the broken line and the distribution in gluon jets, it is observed that the spectrum is softer in gluon jets than in quark jets. The same conclusion can be reached in Fig.9(b).

The LUND and Ali MC's give too hard a spectrum in gluon jets, while the Webber MC gives fairly good description of the data, as seen in Fig.9(b). Further study has been made on this subject by using different kinds of MC's:

1) 2nd order QCD + SF with m fixed, where m is the minimum invariant mass of two partons.

2) 2nd order QCD + SF with y fixed, where $y = m^2/E_{CM}^2$.

3) LLA + CF.

4) LLA + SF.

5) LLA + SF with $G_{ggg} = G_{q\bar{q}g}$, where G_{ggg} and $G_{q\bar{q}g}$ are the coupling constants.

Model 1) gives a distribution of $r(x)$ slightly decreasing as x increases, while model 2) (which is the LUND MC) gives a flat distribution. The difference is due to the fact that the energy dependence of the fraction of multi-parton events is stronger in model 1) than that in model 2). When partons are produced with fixed y, the fraction of events with a given number of partons is almost energy independent, while, when produced with m fixed, the fraction of events with multiple partons increases as E_{CM} increases. Model 3) (which is the Webber MC) and model 4) give almost

the same result, and are consistent with data. The comparison between model 3) and model 4) shows that the ratio $r(x)$ is insensitive to the models of the hadronization, despite the fact that the spectrum itself depends on the hadronization model (see Sec.2.2). Model 5), in which fewer gluons are emitted than in model 4), gives a slightly decreasing distribution, but the decrease is weaker than that of Model 4). The conclusion from these studies is that more partons are required than are provided by a model based on 2nd order QCD.

4 Analysis of 3 jet events

4.1 String effect in 3 jet events

The string effect was first observed by JADE.[39] TPC[40] and TASSO[41] have confirmed this effect. The analysis was done as follows (Fig.10):

- Particles were projected into the event plane.
- 3 Jet events were selected by Sphericity cuts (except for TASSO), and by the clustering algorithm or by the generalized sphericity method.
- The momentum of each jet was calculated by summing vector momenta of particles in the jet, while the energy of each jet was calculated by the opening angles between jets.
- The largest energy jet and the smallest energy jet are called jet 1 and 3, respectively. The probability that jet 3 is the gluon jet was estimated to be around 50% based on a Monte Carlo study.
- Using these 3 jet samples, the following quantities were studied:

    1. The particle and energy flow in the event plane.

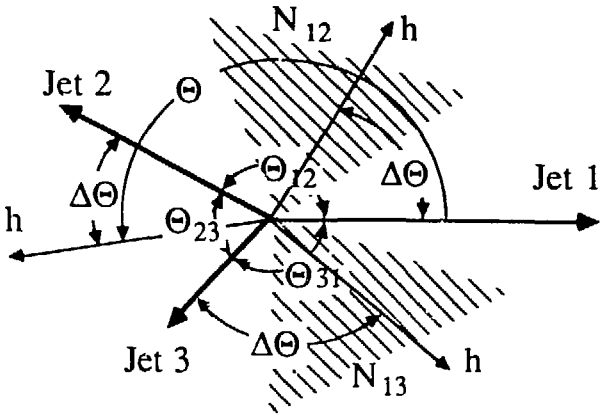

Fig. 10. Definitions of variables in the analysis of 3 jet events.

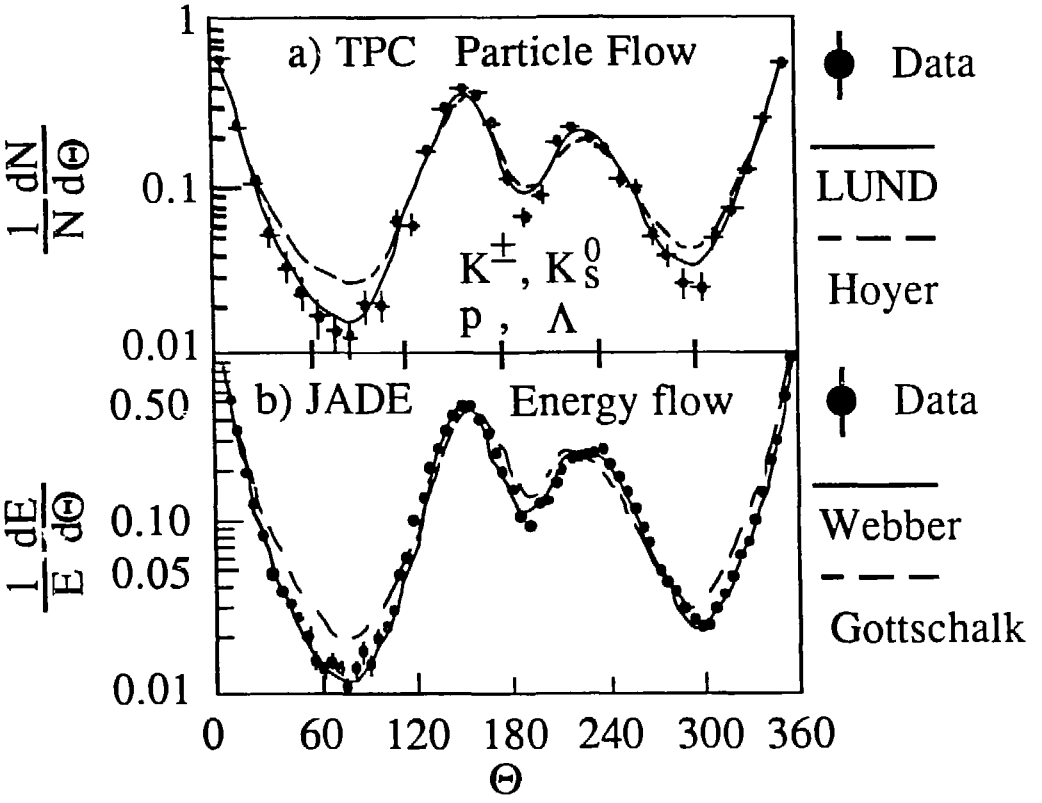

Fig. 11. (a) TPC measurment of heavy particle flow and (b) JADE measurment of energy flow in 3 jet events. Monte Carlo predictions are also given.

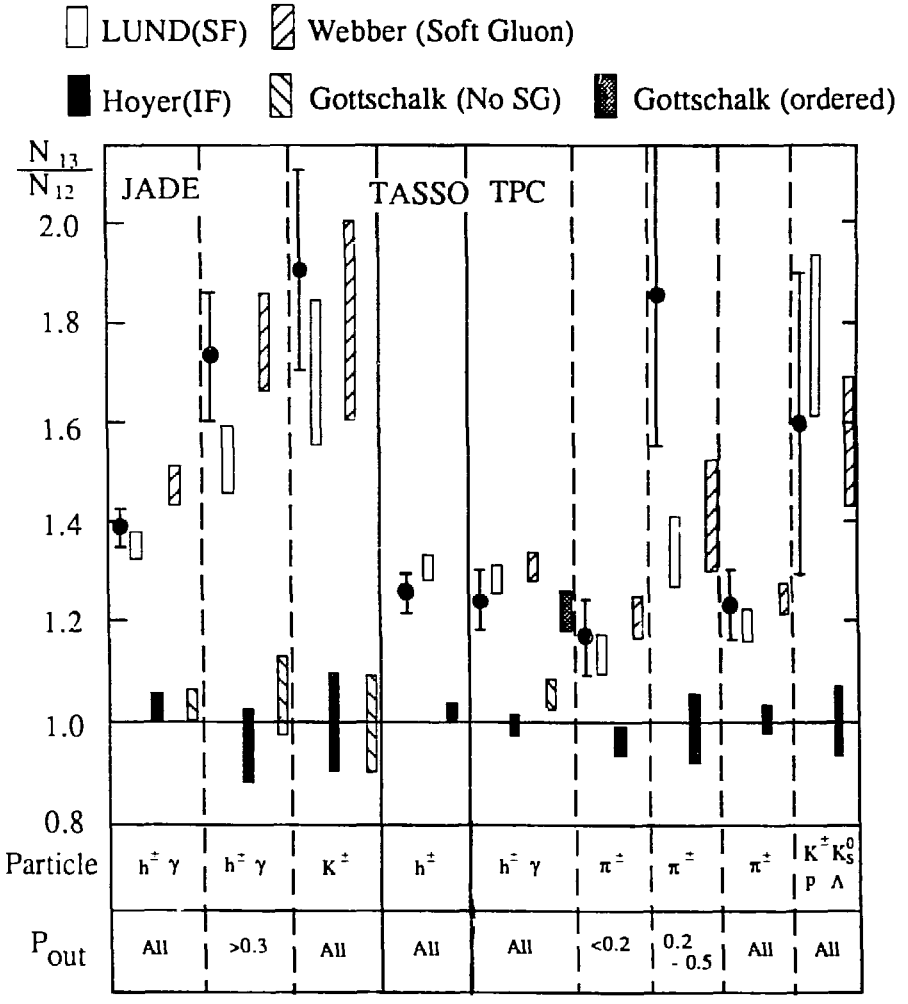

Fig. 12. The ratios N_{13}/N_{12} for different masses and P_{out} of particles. Several MC predictions are also shown. The MC prediction marked by a gray box given by TPC is the Gottschalk MC prediction using only those events in which the angles of partons are ordered (see text).

2. The mass and P_{out} dependence of N_{13}/N_{12}. Here N_{ij} is the number of particles between the jet i axis and the jet j axis with $\Delta\Theta = 0.3 - 0.6 \times \Theta_{ij}$ ($0.25 - 0.75$ for TASSO), and $\Delta\Theta$ is the angle between the jet i axis and the particle and Θ_{ij} is the angle between the jet i axis and the jet j axis.

3. The dependence of N_{13}/N_{12} on the probability of jet 3 being the gluon jet.

Figures 11(a) and (b) show the heavy particle flow by TPC and the energy flow by JADE in the event plane as a function of Θ. Here Θ is the angle of particles in the event plane measured from the direction of jet1 through jet2 to jet3. In Fig.12, N_{13}/N_{12} reported by TPC, JADE and TASSO are plotted for particles with different masses and with different P_{out}, the momentum component out of the event plane. It is clear from Fig.12 that the ratio is larger than unity and more hadrons are produced between jet 1 and jet 3 (quark-gluon) than between jet 1 and jet 2(quark-antiquark). The ratio N_{13}/N_{12} is larger for heavier particles and for particles with larger P_{out}.

In Fig.11 and 12, the predictions by the LUND, Hoyer, Webber and Gottschalk models are also given. Particle distributions predicted by the Hoyer and Gottschalk models do not agree with the measured distributions in the regions between jets, especially between jet 1 and jet 2. These two models predict the ratio N_{13}/N_{12} to be unity, independent of hadron mass and P_{out}. This prediction is common to all IF based models.[39,40] The LUND and Webber models predict N_{13}/N_{12} to be larger than one and to become even larger for heavier particles or larger P_{out}. These predictions are consistent with experimental data.

In order to confirm that this effect is due to the gluon emission, the ratio N_{13}/N_{12} is plotted as a function of the probability that the jet 3 is the gluon

jet by TPC[40] (Fig.13). In this analysis, the probability was calculated as follows. The cross section for $q\bar{q}g$ in 1st order QCD is proportional to $C_{q\bar{q}g}$, where

$$C_{q\bar{q}g} = (x_q^2 + x_{\bar{q}}^2)/(1 - x_q)(1 - x_{\bar{q}}),$$

and x_q and $x_{\bar{q}}$ are the energy fractions of the quark and antiquark. The probability G_{tag}(jet3) is defined as

$$G_{tag}(jet3) = 100 \times C_3/(C_1 + C_2 + C_3),$$

where C_i is the value of $C_{q\bar{q}g}$ when jet i is the gluon jet, using the experimentally determined jet energies. It is clear from this figure that the string effect is enhanced for those events with a higher probability G_{tag}(jet3). The differences between the IF model prediction and the LUND and Webber model predictions are enhanced for those events.

Two different models, LUND and Webber, reproduce the string effect, including the mass and P_{out} dependences of the effect. The common characteristic of these two models is that hadrons are produced from sources moving towards between $q - g$ or between $\bar{q} - g$ in the e^+e^- CM frame. The invariant mass of the source of hadrons depends on the cutoff value of the perturbative phase. The average string mass in the LUND model in the 3 jet sample is around 6 GeV, while the average cluster mass in the Webber model is about 2 GeV; nevertheless both models provide similar predictions for N_{13}/N_{12}.

The soft gluon interference effect, a part of the next to leading order correction, becomes important in the perturbative phase of QCD.[16] Interference terms due to multi-soft gluon emissions cancel a part of the LLA cross section. This effect can be approximately incorporated in Monte Carlo programs by requiring the angles between partons to be ordered, i.e., $\theta_1 > \theta_2$, where θ_1 is

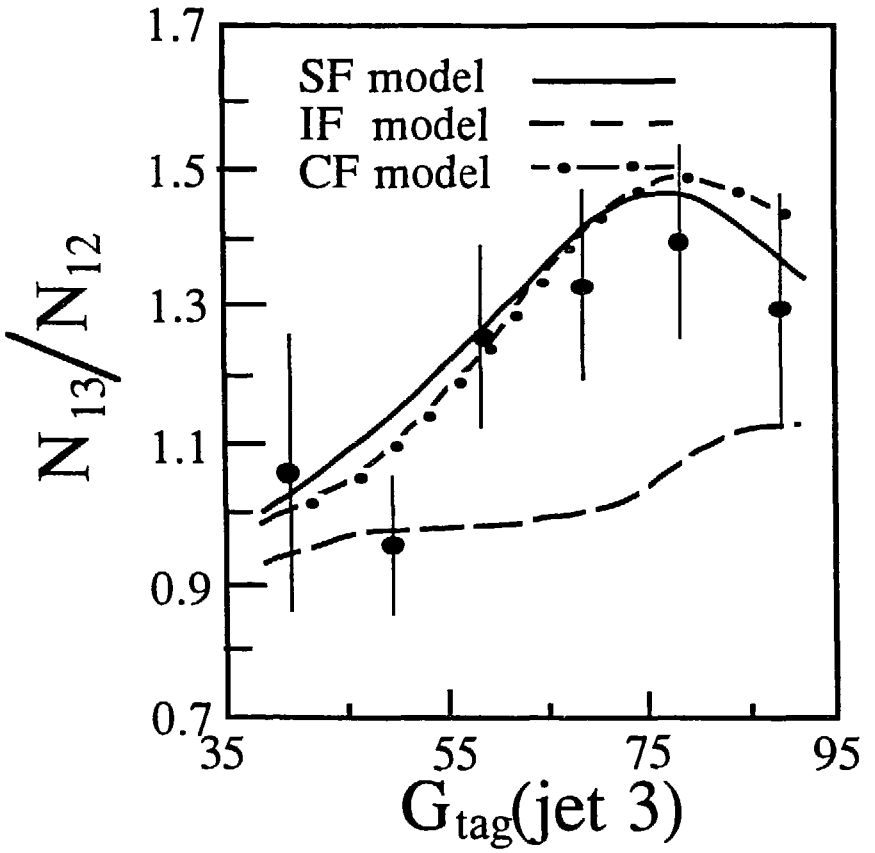

Fig. 13. TPC measurment of the ratio N_{13}/N_{12} as a function of the probability that jet3 is the gluon jet, $G_{tag}(jet3)$.

the angle between the partons preceeding the partons with opening angle of θ_2.[12]

In the Webber model, the angular ordering between partons ensures that partons are more likely to be produced along the direction of the parent parton. This causes depletion of partons between the quark and antiquark jets and depletion of clusters between the quark and antiquark jets. To confirm this point, the ratio N_{13}/N_{12} was calculated using the Gottschalk model, in which soft gluon interference is not included. The Gottschalk model predicts $N_{13}/N_{12} = 1.03 \pm 0.03$. If one uses, however, only those events in which the angles between partons are accidentally ordered, the ratio becomes $N_{13}/N_{12} = 1.22 \pm 0.04$ (See Gottschalk MC predictions in TPC analysis in Fig.12).

4.2 SF vs IF for large momentum particles

The analysis presented above is sensitive to the distribution of hadrons in the central region, which primarily contains small momentum hadrons. TASSO has observed a reversal of the string effect for high momentum particles in the regions between jets, however, i.e., the IF model seems to be favored over SF.[41] Other groups, JADE[42] and TPC[43], have also examined high momentum particles. Neither of them confirmed the above TASSO result.

TASSO has analyzed the data with two methods:

i. The x_{in} dependence of the N_{13}/N_{12} ratio.

ii. The power dependence of the N_{13}/N_{12} ratio.

In the first analysis, the N_{13}/N_{12} ratio was plotted as a function of x_{in}, where $x_{in} = p_{in}/E_{beam}$ and p_{in} is the particle momentum projected onto the

event plane. The data is shown in Fig.14(a) and (b). TASSO has observed that the data points deviate from the prediction of the SF model in the region of $x_{in} > 0.4$, but are consistent with the IF model. The deviation is enhanced when low planarity events are selected, where planarity P is defined to be $P = Q_2 - Q_1$ and Q_2 and Q_1 are medium and smallest eigenvalues of the sphericity tensor. The TPC and JADE data analyzed in an analogous fashion are shown in Fig.14(c) to (e). As can be seen from these figures, the TPC and JADE data are consistent with the SF model predictions at both large and small x_{in} values.

The second analysis by TASSO was done using charged particles as follows:

- Three jet events are selected by the generalized sphericity technique and by requiring that the opening angle between any two jets be larger than 55°.

- The jet axis is then defined by calculating the momentum weighted vector sum

$$\hat{k}_j(n) \propto \sum |p_{in}|^{n-1} \overrightarrow{p}_{in},$$

  where the sum runs over the tracks associated with jet j. The jet axis is determined mainly by small momentum particles for small powers of n and by large momentum particles for large power of n.

- For each power of n, the scaled energy of each jet is calculated by the opening angle between jets, and the jets are labeled 1, 2 and 3 in decreasing order of energy.

- The transverse momentum of jet 3 with respect to the direction of jet 1 is defined to be $x_T(n)$. The difference $\Delta x_T(n) = x_T(2) - x_T(n)$ is used to study the momentum dependence of $x_T(n)$.

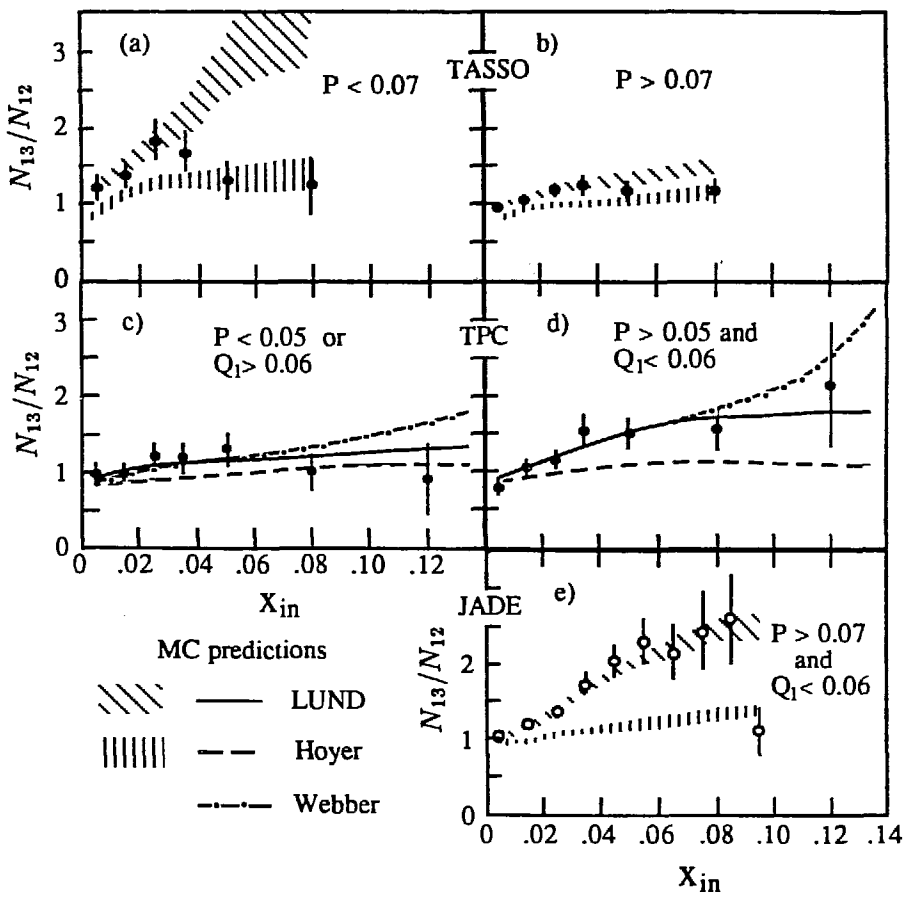

Fig. 14. The ratio N_{13}/N_{12} as a function of x_{in}, measured by TASSO, TPC and JADE. Ranges of P and Q_1 used to select events are shown in the figure. Data are compared with MC predictions.

Figure 15(a) shows the average value of $x_T(n)$ as a function of n. JADE analyzed data in an analogous fashion using charged particles and photons as shown in Fig.15(b). While TASSO did not impose the planarity cut, JADE required planarity cut ($P > 0.07$) and an aplanarity cut($Q_1 < 0.06$). In order to reduce the difference between the TASSO and JADE analyses, events containing more than 3 jets are removed from TASSO data using the clustering algorithm for this plot. The distribution of $\Delta x_T(n)$ is strongly dependent on the analysis, and therefore the n dependence is different from analysis to analysis. In the low n region, the two analyses are in agreement that SF is better than IF. But in the higher n region, the two analyses give different results. The TASSO data points come closer to the prediction of IF for high n region, while the JADE data still favor SF.

The high momentum region is very sensitive to the heavy quark production and the parton production cross sections. More data and further analyses would help to settle the discrepancy between TASSO on the one hand and JADE and TPC on the other.

5 $p - \overline{p}$ correlations and the baryon production mechanism

5.1 Models for baryon production

Several mechanisms for baryon production in e^+e^- annihilation have been proposed. The major models are 1) the diquark model[44] (Fig.16(a)), 2) the popcorn model[45] (Fig.16(b)), and 3) the cluster decay model[46] (Fig.16(c)). In the diquark model, the diquark is considered to be an (effectively) fundamental "particle". The diquark-antidiquark pair is produced from the color field like an ordinary quark-antiquark pair. A baryon is produced by com-

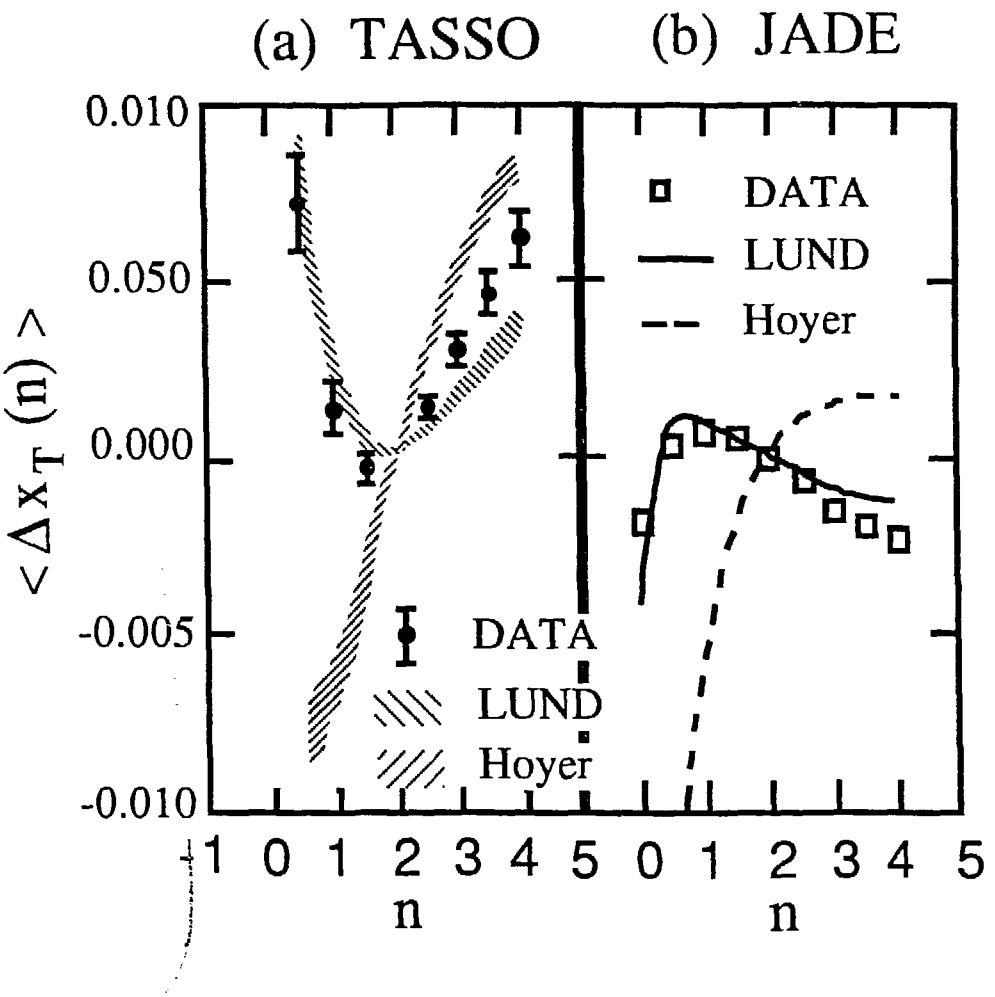

Fig. 15. The difference $\Delta x_T(n)$ as a function of the power n measured by TASSO (a) and by JADE (b). Data are compared with MC predictions.

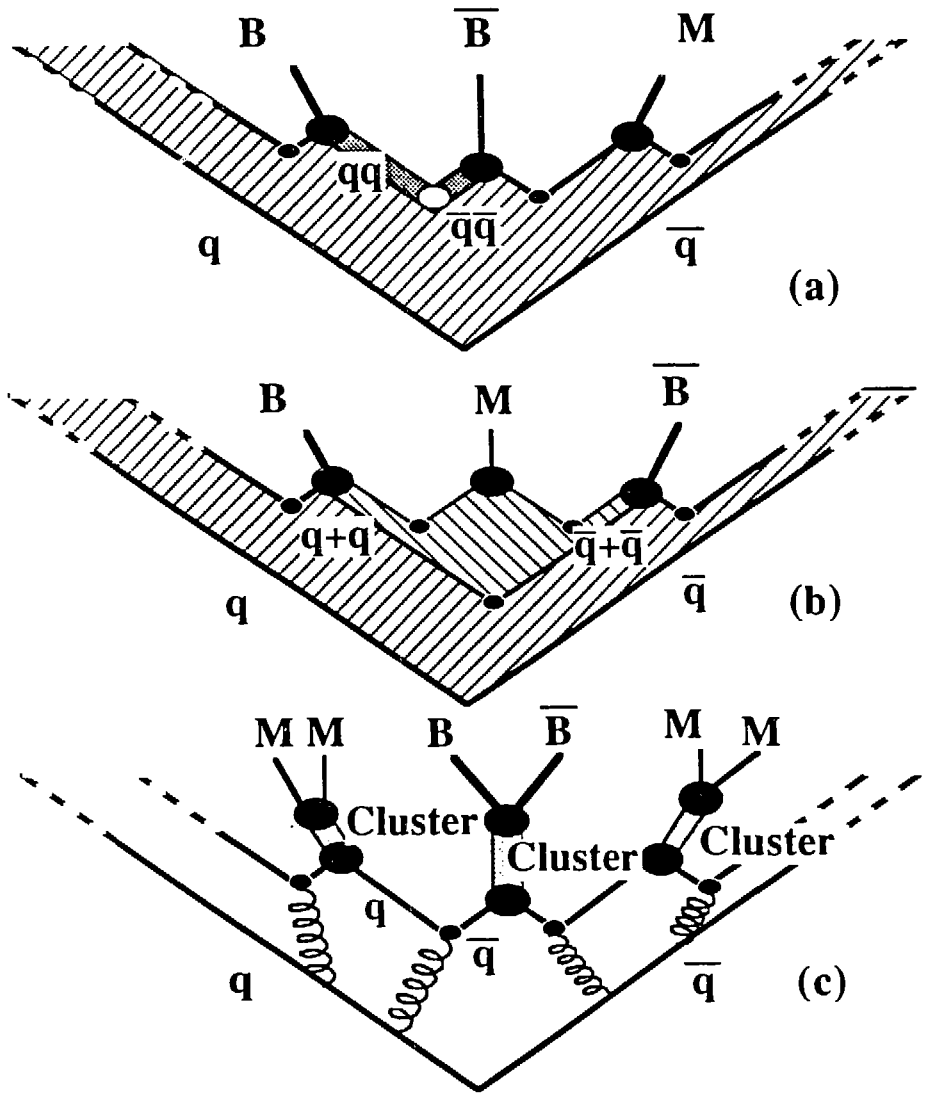

Fig. 16. Schematic representations of baryon production mechanisms in (a) the diquark model, (b) the "popcorn" model and (c) the cluster decay model.

bining a diquark and a quark. The popcorn model was introduced in order to explain baryon production in QCD. In this model, only quark pairs are produced from the color field. It was shown that three quarks can combine themselves to form a color singlet system with a reasonable rate. In the cluster decay model, a baryon pair is produced through the decay of clusters in the same way as a meson pair. In the Webber model, gluons split into quark-anitquark pairs and only mesonic clusters (clusters which contain a quark and an antiquark) appear. A cluster is assumed to decay isotropically into two hadrons in the rest frame of the cluster.

5.2 Cluster decay vs String Model

TPC obtained 110 $p\bar{p}$ and 21 pp, $\overline{p}\overline{p}$ pairs in the proton momentum range of 0.5 to 1.5 GeV, with estimated backgrounds of 7 and 3, respectively. They used this sample to test the above mentioned models.[47] In order to see how the cluster decay model differs from the other two models, the angular distribution of $p\bar{p}$ pairs with respect to the jet axis was studied. The angle θ^* is defined as the angle between the proton momentum and the jet axis in the CM frame of the $p\bar{p}$ pair.

In the cluster decay model, the cluster decays spherically symmetric and the $\cos\theta^*$ distribution is flat. In the diquark model, the proton and antiproton are more likely to be produced along the jet direction because the diquarks are pulled along the direction of the string. The popcorn model gives almost the same prediction as the diquark model for this distribution. The θ^* distribution in the diquark model shows an enhancement around $|\cos\theta^*| = 1$. The predictions of these models in the generator level are shown in Fig.17(a).

In order to remove the contributions of $p\bar{p}$ pairs in which the p and $\bar{p}$ are

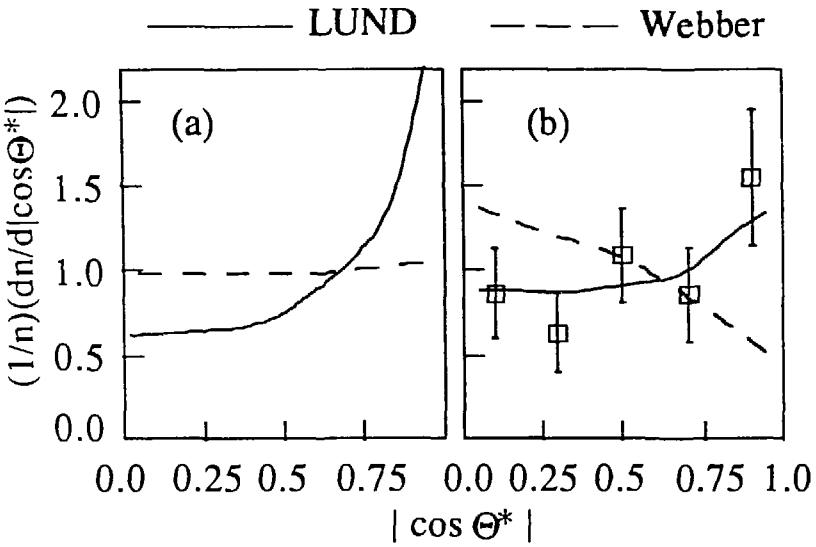

Fig. 17. Distributions of $p - \bar{p}$ pairs in $|\cos\theta^*|$. (a) Predictions of MC's based on CF (Webber, dashed line) and on the diquark model in SF (LUND, solid line) at the generator level, and (b) the TPC data with these two MC predictions.

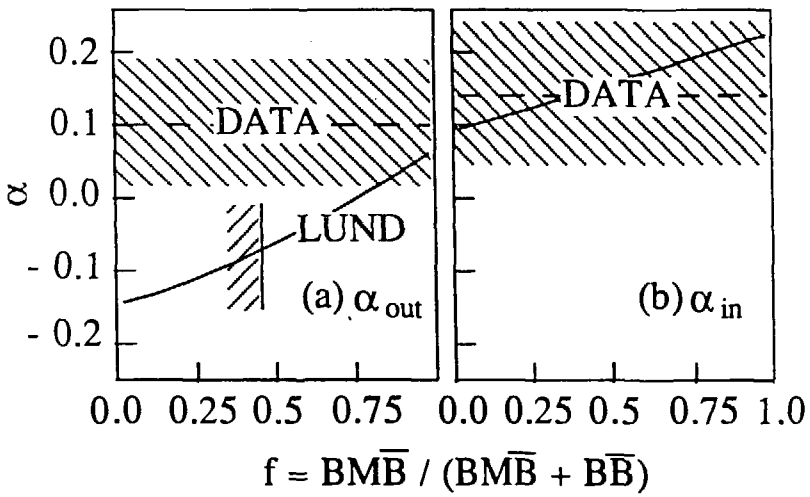

Fig. 18. Correlation coefficiants (a) α_{out} and (b) α_{in} measured by TPC and the popcorn model predictions as a function of the fraction $BM\overline{B}/(B\overline{B} + BM\overline{B})$. The measured values are shown by bands.

produced independently, the θ^* distribution is defined as follows:

$$dn/d|\cos\theta^*| = dn/d|\cos\theta^*|(p+\overline{p}) - dn/d|\cos\theta^*|(p+p, \overline{p}+\overline{p}) \ ,$$

where $dn/d|\cos\theta^*|(p+\overline{p})$ is the distribution of the $p\overline{p}$ pairs and $dn/d|\cos|(p+p, \overline{p}+\overline{p})$ is that of the pp and $\overline{p}\overline{p}$ pairs.

The $|\cos\theta^*|$ distribution measured by TPC is shown in Fig.17(b) together with the predictions of the diquark model and the cluster decay model. The shapes of the distributions suffer from the limited momentum range of p and $\overline{p}$, but the relative difference between the two models is retained. As can be seen from the figure, the data shows an enhancement around $|\cos\theta^*| = 1$. The diquark model reproduces this shape. The cluster decay model, however, shows a decrease at $|\cos\theta^*| = 1$ and is excluded at 95% C.L..

The above result means that baryon pairs are oriented primarily along the jet axis a *la* diquark model prediction and that the the baryon pairs are not produced isotropically in the CM frame of the pair. The implication for the Webber model is that either baryonic clusters, i.e. clusters which contain three quarks, must be introduced or that clusters must decay anisotropically. An updated version of Webber MC (V3.2), which includes baryonic clusters by allowing the splitting of virtual gluons into diquarks, reproduces the enhancement at $|\cos\theta^*| = 1$.

5.3 Diquark model vs Popcorn model

In the diquark model, the baryon and antibaryon are always adjacent, while mesons can be produced between the baryon and antibaryon in the popcorn model. Because of this difference, the correlation between the p and $\overline{p}$ momentum transverse to the jet axis is stronger in the diquark model than in the popcorn model. To measure the strength of this correlation, the

following quantity α is defined using the transverse momenta of the proton $\vec{p_t}(p)$ and the antiproton $\vec{p_t}(\bar{p})$;

$$\alpha \equiv < \vec{p_t}(p) \cdot \vec{p_t}(\bar{p}) > / < \vec{p_t}(p)^2 > .$$

The diquark model predicts $\alpha = -1/2$ at the generator level. In the real analysis, several effects smear this prediction. The largest effect is hard gluon emission. Because of hard gluon emission, the jet axis (sphericity axis) is not the direction of the quark or gluon. To make the analysis less dependent on the gluon emission, two correlation coefficients, α_{out} and α_{in}, are defined from the same equation by using the transverse momentum component out of and in the event plane, respectively.

In order to simulate the popcorn model, a simple mechanism has been incorporated into the LUND MC, whereby baryon pairs are produced with or without a meson between the baryon and the antibaryon.[45] The ratio $f \equiv BM\overline{B}/(BM\overline{B} + B\overline{B})$ is defined as the fraction of baryon pairs with such an intermediate meson. The prediction with $f = 0$ corresponds to the diquark model.

The measured α_{out} and α_{in} are shown in Fig.18(a) and (b). In the same figure, the prediction of the popcorn model is shown as a function of f. This prediction is insensitive to the perturbative part, i.e., the result is almost the same for 2nd order QCD and for the LLA. As can be seen from Fig.18(b), α_{in} suffers from the gluon emission effect and α_{in} is pushed to positive due to the topology of $q\bar{q}g$ events. The model prediction in Fig.18(a) indicates that the value of α_{out} strongly depends on f, i.e., the strength of the correlation between the transverse momentum of p and $\bar{p}$. The data shows a very weak correlation between the transverse momentum of the proton and that of antiproton. From this data, the lower limit on the fraction $BM\overline{B}/(BM\overline{B} + B\overline{B})$ was calculated to be 45% at 90% C.L..

6 Summary

In this presentation recent results on hadron production in e^+e^- annihilation at PEP and PETRA have been summarized with an emphasis on the hadron production mechanism.

In order to understand the hadronization process in the framework of QCD, the questions which need to be answered are 1) how the perturbative phase merges with the non-perturbative phase and 2) how partons in the non-perturbative phase transform into hadrons. The data have been compared with predictions of models based on different assumptions and calculations. For the perturbative phase, parton cross sections are calculated based either on 2nd order QCD or on LLA, possibly with a part of the corrections from the next to leading log. For the non-perturbative phase, hadronization models tested are the independent fragmentation model(IF), the string fragmentation model(SF) and the cluster fragmentation model (CF).

The gluon jet study by MARK II has shown that the particle spectrum in gluon jets is softer than that in quark jets. By comparing the data with the predictions of several Monte Carlo programs, multigluon emission is found to make the spectrum soft. In this case, LLA is a better approximation than 2nd order QCD.

The flavor dependence of the hadronization process is studied by using charm and bottom enriched events tagged by prompt leptons and D*. Available data are consistent with the QCD prediction that hadronization is independent of the quark flavor. Apparent differences in data between heavy quark jets and light quark jets are explained by differences in the momentum spectrum and decay of the first rank hadron. The Monte Carlo based on LLA can explain the difference of the momentum spectrum in heavy quark jets and that in light quark jets by the difference of quark masses, i.e., less

gluons are emitted from heavy quarks than from light quarks.

Cross sections for many kinds of hadrons are fairly well reproduced by a model based on LLA and CF hadronization with only a few fundamental parameters to be adjusted. The SF model, which is very successful in describing hadronization, cannot predict the multiplicities without adjusting several phenomenological parameters. HRS measured the inclusive particle cross section up to $z = 1$. The data are inconsistent with the prediction of the CF model in the region above $z = 0.6$. Another problem with the CF model is its isotropic cluster decay mechanism, as has been pointed out by TPC in $p-\bar{p}$ correlation studies. These problems originate from a simplified treatment of the cluster fragmentation model.

The 3 jet event analysis has proven that the IF model cannot explain the depletion of soft hadrons in the region between the quark and antiquark directions. The SF model explains this signal by the absence of a string between the quark and antiquark. The model with LLA and CF also explains this "string effect" mainly by the soft gluon interference effect. TASSO has reported that the IF model is favored for high momentum hadrons in the region between $q-\bar{q}$. JADE and TPC do not observe this effect, however. Further study is required to determine whether the SF model can reproduce particle distributions in the entire momentum range.

The $p-\bar{p}$ correlation studied by TPC has given the following two results. The observed $p-\bar{p}$ correlation in the polar angle is consistent with the diquark and popcorn mechanisms in the SF model but not consistent with the spherically symmetric decays of clusters incorporated in the CF model. The $p-\bar{p}$ correlation in azimuthal angle is relatively weak, suggesting that a meson pops up between a baryon antibaryon pair at least half of the time.

Acknowledgements

I would like to thank groups who provided new results prior to publication. I am indebted for stimulating discussions to H.-U. Bengtsson, J. Dorfan, J. W. Gary, W. Hofmann, P. Kooijman, A. Petersen, T. Sjoestrand, K. Sugano, and B. R. Webber. T. Kamae, P. Oddone, H. Aihara and E. Wang and other colleagues in the PEP4/TPC collaboration constantly encouraged me in the preparation of the talk and corrected my English in this manuscript. I would also like to express my gratitude to the Program Directors, G. Feldman, F. Gilman and D. Leith for providing me with the chance to give this talk.

References

1. Old data are summarized, for example, by J. Dorfan, Proc. of the 1983 Int. Symp. on Lepton and Photon Interactions at High Energies, Cornell University, Aug. 4-9, 1983, p686; W. Hofmann, Proc. of the Symp. on the High Energy e^+e^- Interactions, Vanderbilt, Tennessee, Apr. 5-7, p329; S. L. Wu, Phys. Rep. 107, 59 (1984).

2. See, for example, E. Reya, Phys. Rep. 69 (1981) 195; A. H. Muller, Phys. Rep. 73 (1981) 237; G. Altarelli, Phys. Rep. 81 1; D. W. Duke and R. G. Roberts, Phys. Rep. 120 (1985) 276; A. H . Muller, talk at the 1985 Int. Symp. on Lepton and Photon Interactions at High Energies, Kyoto, Aug. 19-24, 1985 (this Symp. is refered to as Kyoto Symp. hereafter).

3. S. Glashow, Nucl. Phys. 22 (1961) 579; S. Weinberg, Phys. Rev. Lett. 19 (1967) 1264; A. Salam, Proceedings of the Eighth Nobel Symp. (Almqvist and Wiksells, Stockholm, 1968), p.367.

4. R. K. Ellis, D. Ross and A. Terrano, Phys. Lett. 45B (1980) 1226; Nucl. Phys. B178 (1980) 421; K. Fabricius, G. Kramer, G. Schierholz and I. Schmitt, Phys. Lett. 97B (1980) 431; Z. Phys. C11 (1982) 315; J. Vermaseren, J. Gaemers and S. Oldham, Nucl. Phys. B187 (1981) 301; A. Ali and F. Barreiro, Phys. Lett. B118 (1982) 155; Nucl. Phys. B236 (1984) 269; F. Gutbrod, G. Kramer and G. Schierholz, Z. Phys. C21 (1984) 235.

5. S. Wolfram, XV Recontre de Moriond (1980); R. Odorico, Nucl. Phys. B172 (1980) 157; Phys. Lett. 102B (1981) 341; P. Mazzanti and R. Odorico, Phys. Lett. 95B (1980) 133; Z. Phys. C7 (1980) 61; See also Ref.11, 12 and 13.

6. See, for example, R. D. Field, Proc. of the 1983 Int. Symp. on Lepton and Photon Interactions at High Energies, Cornell University, Aug. 4-9, 1983, p593; T. D. Gottschalk, Lectures at the 19th Int. School of Elementary Particle Physics, Kupari-Dubrovnik, Yugoslavia, 1983.

7. R. Field and R. Feynman, Nucl. Phys. B136 (1978) 1.

8. A. Ali et al., Phys. Lett. B93 (1980) 155.

9. P. Hoyer et al., Nucl. Phys. B161 (1979) 349.

10. B. Andersson et al., Phys. Rep. 97 (1983) 31; T. Sjoestrand, Com. Phys. Comm. 27 (1982) 243; 28 (1983) 229.

11. G. C. Fox and S. Wolfram, Nucl. Phys. B168 (1980) 285; R. D. Field and S. Wolfram, Nucl. Phys. B213 (1983) 65.

12. G. Marchesini and B. R. Webber, Nucl. Phys. B238 (1984) 1; B. R. Webber, Nucl. Phys. B238 (1984) 492.

13. T. D. Gottschalk, Nucl. Phys. B214 (1983) 201; B239 (1984) 325; B239 (1984) 349.

14. T. Sjoestrand, Phys. Lett. 142B (1984) 420.

15. Some problems of the CF model are discussed in T. D. Gottschalk and M. Derrick, Proc. of the 1984 Summer Study on the Design and Utilization of the Superconducting Super Collider, Snowmass, CO (1984).

16. A. H. Muller, Phys. Lett. 104B (1981) 161; Yu. L. Dokshitzer, V. S. Fadin and V. A. Khoze, Phys. Lett. 115B (1982) 242; L. V. Gribov, E. M. Levin and M. G. Ryskin, Phys. Rep. 100 (1983) 1; A. Bassetto, M. Ciafaloni and G. Marchesini, Phys. Rep. 100 (1983) 201; R. Odorico, paper 346 submitted to Kyoto Symp..

17. $\pi^{\pm}$ PEP4/TPC Collab., H. Aihara et al., Phys. Rev. Lett. 52 (1984) 577; TASSO Collab., paper 399 submitted to Kyoto Symp.; HRS Collab., M. Derrick et al., ANL-HEP-PR-85-69, PU-85-537, IUHEE-69, UM HE 85-16 (1985);
π^0 TASSO Collab., R. Brandelik et al., Phys. Lett. 108B, (1982) 71; CELLO Collab., H.J. Behrend et al., Z. Physik C20 (1983) 207; PEP4/TPC Collab., H. Aihara et al., Z. Physik C27, 187 (1985); JADE Collab., W. Bartel et al., DESY 85-029 (Apr. 1985);
ρ^0 TASSO Collab., R. Brandelik et al., Phys. Lett. 117B (1982) 135; JADE Collab., W. Bartel et al., Phys. Lett. 145B (1984) 441;

MARK II Collab., H. Schellman et al., SLAC-PUB-3448, LBL-18391 (Sep. 1984); HRS Collab., M. Derrick et al., ANL-HEP-PR-85-20, PU-85-527, IUHEE-65, UM-HE-85-10 (1985);
$K^{\pm}$ PEP4/TPC Collab., Ref. for $\pi^{\pm}$; MARK II Collab., H. Schellman et al., Phys. Rev. D31 (1985) 3013; TASSO Collab., Ref. for $\pi^{\pm}$; HRS Collab., Ref. for $\pi^{\pm}$;
K_S^0 JADE Collab., W. Bartel et al., Z. Physik C20 (1983) 187; PEP4/TPC Collab., H. Aihara et al., Phys. Rev. Lett. 53 (1984) 2378; TASSO Collab., M. Althoff et al., Z. Physik C27, (1985) 27; MARK II Collab., Ref. for $K^{\pm}$; HRS Collab., Ref. for $\pi^{\pm}$;
K^{*0} PEP4/TPC Collab., Ref. for K_S^0; MARK II Collab., Ref. for ρ^0; HRS Collab., Ref. for ρ^0;
$K^{*\pm}$ JADE Collab., Ref. for ρ^0; MARK II Collab., Ref. for ρ^0;
ϕ PEP4/TPC Collab., H. Aihara et al., Phys. Rev. Lett. 52 (1984) 2201; HRS Collab., M. Derrick et al., Phys. Rev. Lett. 54 (1985) 2568;
η JADE Collab., Ref. for π^0;
$\bar{p}$ PEP4/TPC Collab., Ref. for $\pi^{\pm}$; TASSO Collab., Ref. for $\pi^{\pm}$;
$\bar{\Lambda}$ JADE Collab., W. Bartel et al., Phys. Lett. 104B (1981) 325; PEP4/TPC Collab., H. Aihara et al., Phys. Rev. Lett. 54 (1985) 274; TASSO Collab., Ref. for K_S^0; MARK II Collab., C. de la Vaissiere et al., Phys. Rev. Lett. 54 (1985) 2071; HRS Collab., Ref. for $\pi^{\pm}$;
Ξ^- PEP4/TPC Collab., K. Maruyama, XIX Recontre de Moriond (1984); TASSO Collab., Ref. for K_S^0;
Δ^{++} TASSO Collab., M. Althoff et al., DESY 84-065 (Jul. 1984);
$\Sigma^{*\pm}$ TASSO Collab., Ref. for Δ^{++}; PEP4/TPC Collab., Collab., H. Yamamoto, XX Recontre de Moriond (1985);
Ω^- TASSO Collab., LUND Conference (1984); PEP4/TPC Collab., Ref. for $\Sigma^{*\pm}$.

18. ARGUS Collab., R. S. Orr, EPS Meeting on HEP, Bari, Italy, Jul. 1985.

19. MARK II Collab., H. Schellman et al., Phys. Rev. D31 (1985) 3013; See also Ref. 17.

20. B. Andersson, G. Gustafson and B. Soederberg, Z. Phys. C20 (1983) 317.

21. HRS Collab., M. Derrick et al., ANL-HEP-PR-85-77 (1985).

22. T. D. Gottschalk, private communication.

23. DELCO Collab., H. Yamamoto et al., Phys. Rev. Lett. 54 (1985) 522 and references therein; PEP4/TPC Collab., H. Aihara et al., IS-J-1848.

24. MARK III Collab., A. Duncan, SLAC Summer Inst. on Particle Physics, Jul. 29 - Aug. 6, 1985.

25. Particle Data Group, Rev. Mod. Phys. 56 (1984) No.2.

26. CLEO Collab., T. Bowcock et al., Phys. Rev. Lett. 55 (1985) 923.

27. C. Peterson et al., Phys. Rev. D27 (1983) 105.

28. S. Bethke, paper 325 submitted to Kyoto Symp..

29. M. Suzuki, Phys. Lett. B71 (1977) 139; J. B. Bjorken, Phys. Rev. D17 (1978) 171.

30. MARK II Collab., M. E. Nelson et. al., Phys. Rev. Lett. 50 (1983) 1542; N. S. Lockyer et al., Phys. Rev. Lett. 51 (1983) 1316.

31. MAC Collab., E. Fernandez et al., Phys. Rev. Lett. 50 (1983) 2054; MARK J Collab., B. Adeva et al., Phys. Rev. Lett. 51 (1983) 443; TASSO Collab., M. Althoff et at., Z. Phys. C22 (1984) 219; DELCO Collab., T. Pal et al., CALT-68-1283 (1985).

32. HRS Collab., M Derrick et al., ANL-HEP-PR-85-47 (1985).

33. DELCO Collab., M. Sakuda et al., Phys. Lett. 152B (1985) 399.

34. TASSO Collab., M. Althoff et al., Phys. Lett. 138B (1984) 317.

35. JADE Collab., W. Bartel et al., Phys. Lett. 146B (1984) 121.

36. HRS Collab., P. R. Keston, PhD Thesis in The University of Michigan (1985).

37. H. Yamamoto, talk at Kyoto Symp..

38. MARK II Collab., A. Petersen et al., SLAC-PUB-3759 (1985); MARK II Collab., private communication.

39. JADE Collab., W. Bartel et al., Phys. Lett. 101B (1981) 129; Z. Phys. C21 (1983) 37; Phys. Lett. 134B (1984) 275; paper 379 submitted to Kyoto Symp..

40. PEP4/TPC Collab., H. Aihara et al., Phys. Rev. Lett. 54 (1985) 270; Z. Phys. C28(1985)31.

41. TASSO Collab., M. Althoff et al., paper 400 submitted to Kyoto Symp..

42. JADE Collab., A. Petersen, Private communication.

43. J. W. Gary, PhD Thesis in Lawrence Berkeley Laboratory (1985).

44. B. Andersson, G. Gustafson and T. Sjoestrand, Nucl. Phys. B197 (1982) 45; T. Meyer, Z. Phys. C12 (1982) 77.

45. A. Casher, H. Neuberger and S. Nussinov, Phys. Rev. D20 (1979) 179; B. Andersson, G. Gustafson and T. Sjoestrand, LU TP 84-9 (1984).

46. The Webber Monte Carlo[12] is used in their analysis.

47. PEP4/TPC Collab., H. Aihara et al., Phys. Rev. Lett. 55 (1985) 1047.